

1 Full title

2 Transcriptome of the coralline alga *Calliarthron tuberculosum* (Corallinales, Rhodophyta) reveals
3 convergent evolution of a partial lignin biosynthesis pathway

4

5 Short title

6 *Calliarthron* transcriptomics reveals monolignol biosynthesis pathway

7 Author names

8 Jan Y Xue^{a,*}, Katy Hind^{ab}, Matthew A. Lemay^{ab}, Andrea Mcminigal^a, Emma Jourdain^a, Cheong Xin
9 Chan^c, and Patrick T. Martone^{ab}

10

11 ^a Department of Botany and Biodiversity Research Centre, University of British Columbia, Vancouver,
12 BC, V6T 1Z4, Canada

13 ^b Hakai Institute, Heriot Bay, BC, V0P 1H0, Canada

14 ^c Australian Centre for Ecogenomics, School of Chemistry and Molecular Biosciences, The University of
15 Queensland, Brisbane, Queensland, 4072, Australia

16

17 * Corresponding author: jan.xue@botany.ubc.ca

18

19

20 **Abstract**

21
22 The discovery of lignins in the coralline red alga *Calliarthron tuberculosum* raised new questions about
23 the deep evolution of lignin biosynthesis. Here we present the transcriptome of *C. tuberculosum*
24 supported with newly generated genomic data to identify gene candidates from the monolignol
25 biosynthetic pathway using a combination of sequence similarity-based methods. We identified
26 candidates in the monolignol biosynthesis pathway for the genes 4CL, CCR, CAD, CCoAOMT, and CSE
27 but did not identify candidates for PAL, CYP450 (F5H, C3H, C4H), HCT, and COMT. In gene tree
28 analysis, we present evidence that these gene candidates evolved independently from their land plant
29 counterparts, suggesting convergent evolution of a complex multistep lignin biosynthetic pathway in this
30 red algal lineage. Additionally, we provide tools to extract metabolic pathways and genes from the newly
31 generated transcriptomic and genomic datasets. Using these methods, we extracted genes related to
32 sucrose metabolism and calcification. Ultimately, this transcriptome will provide a foundation for further
33 genetic and experimental studies of calcifying red algae.

34
35 **Keywords:** Red algae, lignification, calcification, transcriptome, gene identification, phenylpropanoid
36 pathway, monolignol

37 38 **Introduction**

39
40 Coralline red algae (Corallinales, Sporolithales, Hapalidiales) are a diverse lineage of calcified seaweeds
41 that play important ecological roles in nearshore ecosystems worldwide: they stabilize coral reefs by
42 creating a calcium carbonate matrix [1–3], induce settlement of invertebrate taxa [4–6], and contribute to
43 the storage of blue carbon through the creation of biogenic calcium carbonates [7,8]. In recent years, there
44 has been increased global attention paid to coralline algae. Taxonomists are clarifying their vastly
45 underestimated species diversity [9–12]; ecologists and physiologists are documenting interspecific

46 variation in coralline growth and calcification, particularly in response to climate stress, which may
47 ultimately impact marine communities [13–17]; evolutionary biologists are examining patterns in
48 coralline trait evolution [18–20] and using >100 million-year-old coralline fossils to strengthen modern
49 phylogenies [21,22].

50

51 The discovery of lignins within cell walls of the coralline species *Calliarthron cheilosporioides*
52 (Corallinales, Rhodophyta) dramatically changed our perspective on the evolution of lignin biosynthesis
53 [23]. Lignins are complex aromatic polymers predominantly found in the secondary cell walls of plant
54 support tissues [24,25] and were long considered to have evolved when land plants emerged from the
55 oceans, enabling upright growth in air [26]. Among the principal chemical components of wood, lignins
56 in plant secondary cell walls help reinforce tissue mechanical properties, permit hydraulic transport, and
57 increase pathogen resistance [27,28]. In the articulated coralline *C. cheilosporioides*, lignins were found
58 predominantly within decalcified flexible joints, called genicula [23], that have remarkable biomechanical
59 properties, permitting this articulated coralline species to thrive along wave-battered coastlines [29,30].

60

61 Because lignin biosynthesis is physiologically complex and involves several enzymes in the monolignol
62 pathway [31–33], Martone et al. [23] proposed that much of the lignin biosynthetic pathway may have
63 predated land plants altogether, evolving in a common ancestor of red and green algae more than one
64 billion years ago. Alternatively, some (or all) of the monolignol biosynthetic pathway may have evolved
65 independently in the embryophyte and rhodophyte lineages. For example, one important enzyme involved
66 in S-lignin production (F5H) evolved independently in lycophytes and embryophytes [34,35]. Moreover,
67 candidate genes related to monolignol biosynthesis have since been found in diverse algal lineages such
68 as diatoms, dinoflagellates, haptophytes, cryptophytes, and green and red algae [36], raising questions
69 about how the monolignol pathway may have evolved across such evolutionarily divergent lineages. Until
70 now, questions about monolignol evolution have largely gone unanswered as transcriptomic and genomic
71 data have mostly been limited to non-coralline red algae (e.g. [37–40] but see [41]).

72

73 Here we present a transcriptome of the articulated coralline *Calliarthron tuberculosum* (a sister species of
74 *C. cheilosporioides*) to investigate the evolutionary history of monolignol biosynthesis. Additionally,
75 though a complete mitochondrial genome [42] and a draft nuclear genome [43] of *C. tuberculosum* were
76 previously published, herein we generated a revised nuclear genome assembly using new short-read
77 sequence data to aid validation of transcriptomic reads. Based on comparative analysis of genome and
78 transcriptome data, we identify gene candidates for a putative monolignol biosynthetic pathway in *C.*
79 *tuberculosum* and investigate evolutionary relationships of these enzymes with those from other
80 taxonomic groups, including their land plant counterparts. We also provide a list of annotated genes in the
81 *C. tuberculosum* transcriptome and a simplified method for extracting genes from metabolic pathways.
82 We illustrate the utility of this dataset by extracting gene candidates involved in sucrose metabolism and
83 calcification. This transcriptomic dataset provides a foundation for future studies of coralline algal
84 ecology, physiology, and evolution.

85

86 **Results**

87

88 *The C. tuberculosum transcriptome is complete and supported by genomic data*

89

90 Two transcriptomic datasets were generated from *Calliarthron* thalli: one from whole tissue (calcified
91 intergenicula plus uncalcified genicula; sample I+G/PTM1 in the deposited data) and a second from
92 intergenicular (i.e., calcified) tissue only (sample I/PTM2). Transcriptome sequencing based on RNA-Seq
93 produced 38.8 total Gb of sequence data (17.3 Gb for sample I+G; 21.5 Gb for sample I). Reads were
94 assembled *de novo* using Trinity. The whole tissue dataset had 172,700,376 total reads and the
95 intergenicular tissue dataset had 215,491,160 total reads with an overall average coverage of 677-fold. A
96 third reference transcriptome combining data from both tissues was assembled independently. All three
97 datasets were combined for subsequent analysis to increase coverage and maximize discovery. The

98 transcriptome data were considered complete based on the recovery of core eukaryotic genes (e.g. 94.5%
99 of CEGMA and 87.8% of BUSCO genes based on TBLASTN; Fig S1A). Genomic sequences were also
100 assembled for *C. tuberculosum* (Table S1), but these remain highly fragmented and were used only as
101 additional support to the transcriptome data in subsequent searches below. More than half (18840; 56.6%)
102 of the 33301 transcripts in the reference transcriptome were supported by the genome data (BLASTN, $E \leq$
103 10^{-5}).

104

105 *The incomplete monolignol biosynthetic pathway in Calliarthron tuberculosum*

106

107 The combined *C. tuberculosum* transcriptomic dataset was searched for genes encoding enzymes from the
108 monolignol biosynthetic pathway. The transcriptomic dataset was translated into all six reading frames
109 and queried with a combination of homology-based approaches, including HMMER searches and KEGG
110 based annotations. Closest homologs from *Arabidopsis thaliana* were also verified (BLASTN, $E \leq 10^{-30}$).
111 We identified gene candidates of 4CL, CCR, CAD, CSE, and CCoAOMT, but not HCT, COMT, PAL,
112 TAL, or PTAL (Fig 1). PAL/TAL/PTAL was considered absent as only fragmented (and no full length)
113 sequences were identified. Evidence for the presence of homologous p450 enzymes (C3H, C3H, and
114 F5H) was weak; as a result, their status was classified as ambiguous (Fig 1). All sequences identified had
115 genomic support (BLASTN, $E \leq 10^{-5}$) except for those identified for PAL/TAL/PTAL.

116

117 **Fig 1. The presence of *C. tuberculosum* sequence candidates in the monolignol pathway.**

118 Red indicates presence of a putative homolog in *C. tuberculosum*; blue indicates no significant hits; green
119 indicates ambiguous presence. Note how the PTAL/PAL/TAL sequences obtained from the HMMER
120 search were indicated as absent as all sequences found were too short, 1/4-1/3 in length relative to those
121 in land plants. All sequences identified have genomic support except for PTAL/PAL/TAL.

122

123 Candidate sequences from *C. tuberculosis* (bolded as contig_gene_isoform in Figs 2, 3, and 4) were
124 characterized by comparing key residues with their land plant homologs in multiple sequence alignments.
125 The evolutionary relationships between the identified *C. tuberculosis* sequences, closely related
126 sequences in additional taxa, and sequences from the broader protein family of their land plant homologs
127 were analyzed in gene trees. Below we describe in detail results for the main biosynthetic enzymes 4CL,
128 CCR, and CAD (Figs 2, 3, and 4). Descriptions of the other biosynthetic enzymes CCoAMT, CSE, and
129 the cytochrome P450 sequences C3H, C4H, F5H are found in Appendix S1 and Figs S2-S4.

130

131 **Fig 2. 4CL candidates from *C. tuberculosis* in relation to plants and other taxa**

132 **(A)** Partial alignment of *C. tuberculosis* candidates (bolded) and embryophyte 4CL sequences. Residues
133 involved in hydroxycinnamate binding are indicated with black triangles [61,62]. Phenylalanine substrate
134 binding pocket is indicated with Box I and Box II.

135 **(B)** Maximum likelihood acyl-activating enzyme (AAE) gene tree showing relationships between
136 *Calliarthron* sequences (magenta dots) and other taxa (Embryophyta – dark green, Chlorophyta – light
137 green, Rhodophyta – red, Animalia and Opisthokonta – purple, Bacteria and Cyanobacteria – blue,
138 Oomycota, Mycetozoa and Fungi – yellow, Ochrophyta – brown). Functionally demonstrated plant 4CLs
139 are labelled (+). Additional functional groups are labelled [44,45]. Ultrafast bootstrap values > 95 are
140 marked by *. Model = WAG+F+G4. Sites with $\leq 80\%$ occupancy were removed. Accession numbers can
141 be found in Appendix S1.

142

143 **Fig 3. CCR candidates from *C. tuberculosis* in relation to plants and other taxa**

144 **(A)** Partial alignment *C. tuberculosis* candidates (bolded) and land plant CCR sequences. Catalytic
145 residues are labelled with NWYCY [64] and additional residues are indicated above with a black box.
146 NADPH binding pocket residues are indicated with black triangles [65] and the GXXGXX[A/G] motif is
147 underlined [66]. Hydroxycinnamonyl binding pocket residues are indicated with a gray triangle [65].

148 **(B)** CCR maximum likelihood gene tree showing relationships between *C. tuberculosis* (magenta dots)
149 and other taxa (Embryophyta – dark green, Chlorophyta – light green, Rhodophyta – red, Animalia and
150 Opisthokonta – purple, Bacteria and Cyanobacteria – blue, Oomycota, Mycetoza and Fungi – yellow,
151 Ochrophyta – brown). Functionally demonstrated plant CCRs are labelled (+). Additional functional
152 groups are labelled. Ultrafast bootstrap values >95 are marked by *. Model = LG+G4. Sites with \leq 80%
153 occupancy were removed. Accession numbers can be found in Appendix S1.

154

155 **Fig 4. CAD candidates from *C. tuberculosis* in relation to plants and other taxa**

156 **(A)** Partial alignment of *C. tuberculosis* CAD sequence candidates (bolded) with land plant CAD
157 sequences. Zn⁺² ion coordinating and proton shuttling residues are indicated with the black triangle,
158 NADPH or NADH interacting residues are boxed. Hydrostatic interaction forming residues are indicated
159 with a black box. Putative substrate-binding residues are indicated with grey boxes. [67–69]

160 **(B)** CAD maximum likelihood gene tree showing relationships between *C. tuberculosis* (magenta dots)
161 and other taxa (Embryophyta – dark green, Chlorophyta – light green, Rhodophyta – red, Animalia and
162 Opisthokonta – purple, Bacteria and Cyanobacteria – blue, Oomycota, Mycetoza and Fungi – yellow,
163 Ochrophyta – brown). Alcohol dehydrogenase (ADH) sequences from yeast, and aldehyde reductase
164 (YAHK and AHR) sequences from *E. coli* were used as the ADH family is closely related to that of CAD
165 [70,71]. Functionally demonstrated plant CADs are labelled (+). Additional functional groups are
166 labelled. Ultrafast bootstrap values >95 are marked by *. Model = LG+G4. Sites with \leq 80% occupancy
167 were removed. Accession numbers can be found in Appendix S1.

168

169 *Identification of 4CL candidates*

170

171 4CL is an acyl-CoA synthase in the monolignol pathway and a member of the acyl-activating enzyme
172 (AAE) superfamily. 4CL converts p-coumaric acid, caffeic acid, and ferulic acid into their respective
173 hydroxycinnamoyl-CoA thioesters. We identified 11 candidate 4CL-coding transcripts: two based on

174 KEGG analysis and nine additional sequences based on HMMER searches (Fig 2A). A query of these
175 sequences against the *A. thaliana* proteome returned related proteins within the acyl-activating enzyme
176 superfamily but not the *A. thaliana* 4CL (Table S2). Moderate sequence conservation exists in substrate
177 binding and hydroxycinnamate binding residues between 4CL candidates in *C. tuberculosum* (bolded)
178 and 4CLs in land plants (identity similarity [IS] > 70% Fig 2A).

179
180 In the 4CL gene tree analysis, most *C. tuberculosum* sequences grouped with sequences from other
181 Rhodophytes (Fig 2B). In addition, *C. tuberculosum* sequences grouped within several functional clades
182 including malonate CoA ligase (ultrafast bootstrap support [BS] = 100%), succinylbenzoate CoA ligase
183 (BS = 87%), oxylate CoA ligase (BS = 100%), acetyl CoA synthase (BS = 100%), and the long chain
184 fatty acid CoA ligase (BS = 89%) (magenta dots, Fig 2B) [44,45]. In contrast, embryophyte 4CL
185 sequences form a clade separated from candidate 4CL sequences in *C. tuberculosum* (BS = 99% Fig 2B)
186 by the luciferase containing outgroup. Thus, 4CL candidates in *C. tuberculosum* did not show any clear
187 homology to functionally demonstrated 4CL sequences from embryophytes.

188

189 *Identification of CCR candidates*

190

191 CCR is the first committed enzyme in the monolignol pathway, reducing cinnamoyl-CoA esters to
192 cinnamaldehydes. We identified three sequences as candidate CCR-coding transcripts: one based on
193 KEGG analysis and two additional sequences based on HMMER searches (Fig 3A). A query of these
194 sequences against the *A. thaliana* proteome returned sequences within the CCR family (CCR7, CCR4,
195 CCR-Like6) (Table S2). Substrate-binding residues (NWYCY) and the hydroxycinnamonyl-binding
196 pocket showed low sequence conservation (IS <80%). In contrast, the core catalytic residues (S, T, and
197 K) and NADPH-binding residues appear to be conserved (IS >90%) between the candidate sequences in
198 *C. tuberculosum* and CCRs in land plants (Fig 3A).

199

200 In the CCR gene tree analysis, *C. tuberculosum* sequences varied in their relatedness to other taxa with
201 some sequences closer to Rhodophytes and others more closely related to Oomycota/Mycetozoa/Fungi
202 (Fig 3B). Additionally, CCR candidates in *C. tuberculosum* were mapped with epimerase dehydratase
203 type sequences that included the *A. thaliana* CCR family (Fig 3B). Sequences from *C. tuberculosum*
204 grouped with epimerase dehydratase type sequences of non-embryophyte origin. In contrast, embryophyte
205 CCR, class 2 CCR, and CCR-like form an independent clade (BS >97%). The embryophyte CCR clade
206 and the non-embryophyte epimerase dehydratase clade (containing sequences from *C. tuberculosum*)
207 were more closely related than the embryophyte dihydroflavonol-4-reductase protein (DFR) group within
208 the overall epimerase dehydratase family.

209

210 *Identification of CAD candidates*

211

212 CAD, the final step in the monolignol pathway, is an alcohol dehydrogenase converting various
213 hydroxycinnamaldehydes to their respective hydroxycinnamyl alcohols. SAD, proposed to catalyze this
214 same reaction for sinapyl monolignols [46], is added into our analysis despite debate over their function.
215 We identified five sequences as candidate CAD-encoding transcripts: two based on KEGG analysis and
216 three additional sequences based on HMMER searches (Fig 4A). A query of these sequences against the
217 *A. thaliana* proteome returned CAD2 and other alcohol dehydrogenases (Table S2). NADPH-binding
218 motifs show moderate conservation (IS >80%) (Fig 4A). One *C. tuberculosum* sequence showed high
219 conservation with land plant counterparts, suggesting a promising CAD candidate (+ in Figs 3A and 3B).

220

221 In the CAD gene tree analysis, all *C. tuberculosum* sequences grouped with sequences from other
222 Rhodophytes (Fig 4B). CAD candidates in *C. tuberculosum* were mapped with their embryophyte CAD
223 counterparts and closely related alcohol dehydrogenases. Sequences from *C. tuberculosum* grouped
224 together with oxidoreductases (BS = 100%), sorbitol dehydrogenases (BS = 100%), general alcohol
225 dehydrogenases (BS = 100%), and an algal CAD clade (BS = 100%). Sequences in this algal CAD clade

226 were based on previous sequence similarity-based annotation and have not been functionally
227 demonstrated. In contrast, the land plant CAD and SAD sequences form their own clades (BS 100%; Fig
228 4B) that are separated from the *C. tuberculosum* candidates by the functionally distinct alcohol
229 dehydrogenases, such as yeast alcohol dehydrogenase 7 (ADH7) and *E. coli* aldehyde reductase (YAHK).

230

231 *Identification of additional metabolic pathways in Calliarthron tuberculosum*

232

233 To enable broad and rapid identification of *C. tuberculosum* genes involved in specific metabolic
234 processes, we present two general tools for gene identification within the *C. tuberculosum* transcriptome
235 dataset using KEGG based annotations. This involves extracting whole metabolic pathways or individual
236 genes (see Appendix S1; Fig S5). We included annotations for all metabolic genes recovered in the *C.*
237 *tuberculosum* transcriptome (Table S3). We identified 36 putative *C. tuberculosum* genes present in the
238 starch and sucrose metabolism pathway (Fig S5; Table S4). In addition, we individually searched for
239 genes potentially involved in calcification [41,47,48] and identified 13 sequence candidates related to
240 calcium transport, six related to inorganic carbon transport, five related to pH homeostasis, 19 putative
241 carbonic anhydrases, and 12 putative HSP90 genes (Table S5).

242

243 **Discussion**

244

245 *Evidence for convergent evolution of monolignol biosynthesis*

246

247 Using sequence similarity methods with genes from the monolignol pathway in land plants, we identified
248 candidates for five genes related to monolignol biosynthesis (4CL, CCR, CAD, CCoAOMT, and CSE)
249 from the newly generated *C. tuberculosum* transcriptomic dataset. These gene candidates are supported
250 by genomic evidence, retain major motifs from their respective gene family, and return their *A. thaliana*

251 counterpart in reciprocal BLAST analyses, suggesting that these enzymes may function similarly in
252 monolignol biosynthesis in *C. tuberculosis*.
253
254 Despite supporting evidence from sequence similarity analyses, functional predictions for candidate
255 sequences in the monolignol pathway within *C. tuberculosis* are obscured by the gene tree analysis. If
256 the monolignol pathway in embryophytes and *C. tuberculosis* evolved in a common ancestor and was
257 retained through conserved evolution, we would expect their sequences to form functional clades
258 uninterrupted by functionally divergent protein sequences. However, with the exception of the
259 CCoAOMT candidate, our gene tree analyses consistently showed that monolignol biosynthetic genes in
260 land plants are not sister to those in *C. tuberculosis*. *C. tuberculosis* sequences were found within each
261 respective overall protein family, but consistently grouped with land plant genes of non-monolignol
262 forming function. If these *C. tuberculosis* sequences are functionally homologous to the monolignol
263 biosynthesis counterpart in land plants, then they likely arose independently in *C. tuberculosis*.
264 Convergent evolution in protein function, with phylogenetic patterns of protein sequences with similar
265 functions intersected by sequences with dissimilar functions, is not uncommon in cell wall synthesizing
266 enzymes [49]. Biosynthetic enzymes in *C. tuberculosis* could have evolved similar substrate specificity
267 after the divergence of red algae and land plants or, alternatively, may reflect genes that were individually
268 acquired. Previous evidence suggests that the core monolignol biosynthesis genes (4CL, CCR, and CAD)
269 in *C. tuberculosis* may have been acquired through horizontal gene transfer from a bacterial source [36].
270 Thus, over evolutionary time genes in *C. tuberculosis* may have developed enough synchronicity in gene
271 expression and protein regulation to produce an ad hoc monolignol biosynthetic pathway.
272
273 Alternatively, the phylogenetic evidence might suggest that gene candidates in *C. tuberculosis* do not
274 function in monolignol biosynthesis and instead have a function similar to their sister sequences within
275 their distinct phylogenetic groupings. For example, considering only clustering patterns in the
276 phylogenetic data, perhaps *C. tuberculosis* contig 141618 functions as a CoA ligase that acts on

277 malonate and not coumarate (4CL enzyme) (Fig 2B). However, the tandem use of stricter curated
278 sequences in our predictive HMM models and more flexible HMM models with previously annotated
279 data, such as KEGG annotations, improves our confidence in finding potential gene candidates.
280 Biochemical or functional assays will ultimately be needed to verify the function of candidate gene
281 sequences.

282

283 *The monolignol biosynthesis pathway and missing steps in Calliarthron tuberculosis*

284

285 Several key steps in the monolignol biosynthetic pathway were not recovered in the *C. tuberculosis*
286 transcriptome, including PAL, TAL, PTAL, HCT, COMT, C3H, C4H, or F5H. Although we cannot
287 dismiss that these observations may be due to fragmented sequences in the assembled genome and
288 transcriptome data, we present several other possibilities.

289

290 The ammonia-lyase PAL, TAL, or PTAL creates the first substrates in the monolignol biosynthetic
291 pathway [50–52]. Although no full-length homologs were identified in the *C. tuberculosis*
292 transcriptome, short sequence candidates identified may represent a fragmented gene. However, these
293 short sequences lacked genomic support, indicating they may be contaminants of non-*Calliarthron* origin.
294 For this reason, PAL, TAL, and PTAL are currently indicated as absent (Fig 1). If these are indeed from
295 *C. tuberculosis*, RACE amplification could help determine if the short ammonia-lyase we identified has
296 a longer transcript. *C. tuberculosis* likely has an ammonia-lyase acting on phenylalanine or tyrosine
297 since PAL and TAL are also key enzymes in producing flavanoids and coumarins, which have been
298 previously detected in both fleshy and coralline red algae [53]. Further validation will be required to
299 elucidate their presence.

300

301 C3H, C4H, or F5H are p450 monooxygenases responsible for converting substrates across the monolignol
302 pathway eventually resulting in H to S to G type monolignols, respectively (Fig 1). P450 sequence

303 candidates have been identified, but their substrate-specific identity as C3H, C4H, or F5H homologs is
304 unclear. The cytochrome P450 sequence candidates from the *C. tuberculosum* transcriptome form two
305 divergent groups. One group is likely involved in carotenoid biosynthesis, positioned within the CYP97
306 clade, while the other group forms their own clade of unknown function (Fig S2B). The identified
307 candidates from *C. tuberculosum* may have multi-substrate specificities, acting on various substrates,
308 including monolignol intermediate products. Some substrate promiscuity has previously been observed
309 within members of the cytochrome P450 enzyme family [54,55]. Alternatively, each of the identified
310 P450 clades in *C. tuberculosum* could contain a new class of cytochrome P450 capable of functioning in
311 H-, G-, or S- unit monolignol biosynthesis. This proposed convergent evolution of a distinct and
312 independently-evolved cytochrome P450 involved in monolignol production has previously been
313 documented in the clubmoss *Selaginella moellendorffii* (F5H) [34,35]. In any case, the presence of unique
314 P450s represents an interesting avenue of exploration to elucidate substrate specificity and functionality
315 in the monolignol pathway in *C. tuberculosum*.

316
317 HCT is one alternative route shifting monolignol synthesis from H- to G- to S- types using a temporary
318 shikimate decoration (Fig 1) [56]. Its absence could suggest that *C. tuberculosum* does not utilize an HCT
319 enzyme or create G lignin using this route. Another alternative route in G- and S- type monolignol
320 synthesis utilizes a CSE enzyme that acts on caffeoyl shikimate, an HCT downstream product (Fig 1).
321 The absence of an HCT is at odds with the CSE enzyme identified in this study (Fig 1), suggesting that
322 the CSE candidate identified may not be utilized in the monolignol biosynthetic pathway for *C.*
323 *tuberculosum*. Though this absence could be due to fragmentation in the transcriptome, more data are
324 required for further validation.

325
326 COMT is necessary for S type monolignol production in angiosperms [57–59]. The absence of this
327 enzyme raises questions about how *C. tuberculosum* can produce sinapyl alcohol, a precursor component
328 for S monolignols. Some evidence exists for a bifunctional enzyme in pine that can function as both

329 COMT and CCoAOMT (named AEOMT) in heterologous systems [60]. However, only moderate-to-low
330 sequence similarity is shared among CCoAOMT, COMT, and the bifunctional AEOMT. Perhaps a
331 similar protein with broad substrate specificity is present in *C. tuberculosis* but has yet to be identified
332 based on sequence similarity.

333

334 **Conclusion**

335

336 In summary, we have identified several gene candidates in the *C. tuberculosis* transcriptome that
337 represent central components in the monolignol biosynthetic pathway, helping to explain the surprising
338 presence of lignins in this coralline red alga. Despite the complexity of monolignol biosynthesis, and
339 contrary to the predictions outlined in Martone et al. [23], our gene trees do not demonstrate a deeply
340 conserved evolution of monolignol biosynthesis, but instead suggest that each of the enzymes identified
341 in *C. tuberculosis* likely evolved independently from those found in land plants. Interestingly, there
342 remain several key enzymes in the monolignol pathway whose sequences have not been identified,
343 including those related to pathway entry and to shifting the types of monolignols produced that would
344 form H-, G-, and S-lignins within the cell wall. Further biochemical evidence and validation of sequence
345 expression will be necessary to provide functional support for both the genes identified and to elucidate
346 potential alternative routes in the monolignol biosynthetic pathway in *C. tuberculosis*. By providing
347 methods to easily identify additional gene candidates from the *C. tuberculosis* transcriptome, we aim to
348 facilitate future research on this fascinating organism.

349

350 **Methods**

351

352 **Data and code availability**

353

354 All sequencing data generated from this study are available at European Nucleotide Archive
355 (transcriptome data: accession PRJEB39919; genome data: accession PRJEB39919). Genome supported
356 transcripts, transcriptome assemblies, annotations, and an example of metabolic pathway extraction are
357 available on Github (<https://github.com/martonelab/geneAnnotCalliarthronTranscriptome/>).

358

359 **Experimental model and subject details**

360

361 *Specimen collection and sequencing*

362

363 Two male, haploid specimens of *Calliarthron tuberosum* were collected October 6, 2013, from
364 Bluestone Point (48.81952, -125.1640), Bamfield, British Columbia, Canada and verified as haploid male
365 specimens by microscopy. A portion of each collected sample was pressed and deposited into the UBC
366 herbarium with voucher codes A89970 and A89985. Voucher codes can be queried at
367 <https://herbweb.botany.ubc.ca/herbarium/search.php?Database=algae> for more information.

368 Calcified intergenicula and non-calcified genicula from each individual were divided into two portions for
369 data collection: either whole tissue (Sample I+G/PTM1 in the dataset) or calcified tissue only (Sample
370 I/PTM2 in the dataset). Total RNA was extracted using the Spectrum Plant Total RNA kit (Cat #
371 STRN50, Sigma-Aldrich) and sequenced on the Illumina HiSeq 2000 platform (paired-end 2x100bp,
372 insert size ~220bp).

373

374 *Abbreviation of enzyme names*

375

376 CAD, (hydroxy)cinnamyl alcohol dehydrogenase; SAD, sinapyl alcohol dehydrogenase; CCoAOMT,
377 caffeoyl-CoA O-methyl transferase; CCR, (hydroxy)cinnamoyl-CoA reductase; C3'H, p-coumaroyl
378 shikimate 3'-hydroxylase; C4H, cinnamate 4 hydroxylase; 4CL, 4-hydroxycinnamoyl-CoA ligase;
379 COMT, caffeic acid O-methyltransferase; F5H, ferulic acid/coniferaldehyde/coniferyl alcohol 5-

380 hydroxylase; HCT, hydroxycinnamoyl-CoA:shikimate hydroxycinnamoyl transferase; PAL,
381 phenylalanine ammonia-lyase

382

383 *Transcriptome assembly and annotation*

384

385 Illumina sequence reads were assembled using Trinity with the *de novo* mode at default setting [72],
386 independently for each anatomical sample (I+G/PTM1 ; I/PTM2 in the ENA database). A reference
387 transcriptome was also assembled *de novo* using Trinity by independently combining the sequence reads
388 generated from both samples. The assembled transcripts were annotated using Blast2GO [73]. Briefly,
389 each transcript was searched against the NCBI RefSeq protein database (BLASTX, $E \leq 10^{-5}$), and its
390 putative function was inferred based on the top protein hit and Gene Ontology (GO) terms. These proteins
391 were then mapped onto the corresponding metabolic pathways in the Kyoto Encyclopaedia of Gene and
392 Genomes (KEGG) database [74]. Identification of genes present in KEGG annotated pathways were
393 extracted using the pathview package [75].

394

395 *Filtering contaminant sequences in genome assembled data*

396

397 To identify putative contaminant sequences in the genome assembly, each genome scaffold was searched
398 (BLASTN) against a database of archaeal, bacterial and viral genome sequences retrieved from the NCBI
399 RefSeq database. Sequences with a significant hit ($E \leq 10^{-5}$, covering > 50% of the query length) were
400 considered putative contaminants and removed from the genome assembly. To identify broad differences
401 in sequence characteristics, genomic scaffolds with and without transcriptomic support were compared
402 for G+C content and transcript length (Fig S1B). Scaffolds with no transcript support and low recovery of
403 eukaryotic genes (< 6% BUSCO or CEGMA recovery) were also identified as likely putative
404 contaminants and removed from the genome assembly.

405

406 *Genome annotation guided by transcriptome evidence*

407

408 Repetitive elements in the genome assembly were identified and masked using RepeatMasker version

409 open-4.0.6 [76]. To maximize recovery of transcript support for genome scaffolds, the transcriptomes

410 (I+G/PTM1; I/PTM2 in the dataset) were mapped against the masked genome scaffolds using PASA

411 v2.0.2 [77], and full-length coding sequences (CDSs) were predicted with TransDecoder v5.0.1 [72].

412 These CDSs represent the primary set of putative genes and were used as extrinsic hints to guide *ab initio*

413 gene prediction using AUGUSTUS v3.2.1 [78] from the genome scaffolds.

414

415 *HMM based gene candidate search*

416

417 Monolignol biosynthesis gene candidates were identified from the *C. tuberculosum* transcriptomic dataset

418 using Hidden Markov Model (HMM) based searches [79]. Transcriptomic sequence contigs were

419 translated into all six reading frames using EMBOSS Transeq [80]. This amino acid database was used

420 for subsequent sequence searches. HMM profiles used to search for homologs in the transcriptome were

421 produced by aligning amino acid sequences of a given protein or protein family using MUSCLE [81] with

422 no manual adjustment. The profiles were searched against the translated *C. tuberculosum* dataset in

423 HMMER searches [79] to look for putative sequence homologs. Sequences more than 100 amino acids

424 long were retained for subsequent analysis. These sequences were then searched against the *Arabidopsis*

425 (GenBank taxid:3701) proteome using NCBI's BLAST [82] to verify their closest homolog match

426 (BLASTP, $E \leq 10^{-30}$).

427

428 *Domain and motif comparison*

429

430 The monolignol biosynthetic genes and their overall gene families contain sequence domains that

431 influence protein shape and function. To compare these key domains, multiple sequence alignments

432 (MSA) of candidate amino acid sequences from *C. tuberculosis* with their land plant counterpart protein
433 were produced. Sequences were aligned using MUSCLE under default settings [81]. Key domains and
434 motifs were chosen based on available literature and highlighted in the MSA as indicated in each figure
435 legend. In each MSA, an asterisk (*) represents full conservation; and a period (.) represents sites with
436 conservation >50%. Accession numbers can be found in Appendix S1.

437

438 *Gene tree analysis*

439

440 Gene trees were reconstructed for the candidate sequences of *C. tuberculosis* identified. For each gene
441 tree analysis, sequence candidates from *C. tuberculosis*, the functionally demonstrated enzyme sequence
442 from land plants, enzyme sequences from the overall protein family from land plants, and the top 20
443 sequences identified by NCBI BLAST using *C. tuberculosis* candidates as a query against the total
444 database using default settings (BLASTP, $E \leq 10^{-20}$) were compiled. Land plant sequences identified to
445 represent the functional gene and overall gene family were curated by a literature search. For each set of
446 sequences, a multiple sequence alignment was performed using MUSCLE with default setting [81]. Sites
447 with <80% coverage were removed using trimAl [83]. IQTree was used to search for the evolutionary
448 model alignment under a BIC criterion [84,85]. A maximum likelihood tree was reconstructed using
449 IQTree [86], with node support calculated based on 1000 ultrafast bootstrap pseudoreplicates in IQTree
450 [86]. A clade is considered strongly supported when bootstrap value $\geq 95\%$. FigTree was used to edit
451 branch width and colors [87]. Accession numbers can be found in Appendix S1.

452

453 *Generation of genome data as additional support for transcriptome data*

454

455 Genome data of *C. tuberculosis* were generated using Illumina Iix platform (paired-end 2×150 bp reads,
456 insert size ~ 350 bp). An overview of the summary statistics for the genome assembly can be found in
457 Table S1. Adapter sequences were removed using Trimmomatic v0.33 [88] (LEADING:25

458 TRAILING:25 HEADCROP:10 SLIDINGWINDOW:4:20 MINLEN:50). The generated filtered
459 sequence reads and the previously published genome data (GenBank accession #: SRP005182) generated
460 using the 454 pyrosequencing platform [43] were used in a *de novo* genome assembly using SPAdes [89].
461 The 454 reads were treated as unpaired, single-end reads in the assembly process. This *de novo* assembly
462 was further scaffolded with the transcriptome data using the L_RNA_Scaffolder [90]. Putative
463 contaminant sequences were removed based on shared similarity against known genome sequences from
464 bacterial, archaeal, and viral sources in NCBI RefSeq (BLASTN, $E \leq 10^{-5}$), and subsequently based on
465 discrepancy in G+C content of the assembled scaffolds, and the recovery of core eukaryotic genes
466 (CEGMA and BUSCO). Because the genome assembly is fragmented, genome scaffolds on which no
467 transcripts were mapped were filtered out, yielding the final genome assembly (21,672 scaffolds, total
468 bases 64.15 Mbp). These genome scaffolds were used as additional support for the transcriptome data.
469 For the reference transcriptome (combined I+G/PTM1 ; I/PTM2), putative coding sequences were
470 predicted based on alignment of the assembled transcripts against the genome scaffolds using PASA [77]
471 and TransDecoder [72], from which the coded protein sequences were predicted.

472

473 *Completeness of transcriptome and genome data*

474

475 The completeness of the genome and transcriptome data was assessed by the recovery of core conserved
476 eukaryote genes with the Core Eukaryotic Genes Mapping Approach (CEGMA) [91] and Benchmarking
477 Universal Single-Copy Orthologs (BUSCO) [92] datasets. CEGMA and BUSCO datasets (eukaryote
478 odb9 and Viridiplantae odb10) were independently used as query to search against the predicted proteins
479 from the reference transcriptome (combined IG and IO) using BLASTP ($E \leq 10^{-5}$) and against the same
480 transcriptome using TBLASTN ($E \leq 10^{-5}$). The core CEGMA and BUSCO proteins were also queried
481 against the 21,672 genome scaffolds using TBLASTN ($E \leq 10^{-5}$).

482

483

484 **Key Resources Table**

485

REAGENT or RESOURCE	SOURCE	IDENTIFIER
Biological Samples		
<i>Calliarthron tuberculosum</i> (sample vouchers)	This paper	A89970 and A89985 at https://herbweb.botany.ubc.ca/herbarium/search.php?Database=algae
Critical Commercial Assays		
HiSeq 2000 (Transcript reads)	Illumina	
Iix platform (Genomic reads)	Illumina	
Spectrum Plant Total RNA kit	Sigma-Aldrich	STRN50
Deposited Data		
Raw sequencing reads for transcriptomic and genomic data	This paper	PRJEB39919
Genome supported transcripts, transcriptome assemblies, annotations	This paper	https://github.com/martonelab/geneAnnotCalliarthronTranscriptome/
Additional <i>Calliarthron</i> Genomic Reads	[43]	SRP005182
<i>Pyropia</i> genomic data	[39]	MXAK00000000
<i>Arabidopsis</i> Proteome		taxid:3701

Software and Algorithms		
TransDecoder v5.0.1	[72]	https://github.com/TransDecoder/wiki
Trinity	[72]	https://github.com/trinityrnaseq/wiki
Blast2GO	[73]	https://www.blast2go.com/
Kyoto Encyclopedia of Genes and Genomes (KEGG)	[74]	https://www.genome.jp/kegg/
Pathview R Package	[75]	https://www.bioconductor.org/packages/release/bioc/html/pathview.html
HMMER	[79]	http://hmmerrg.org/
EMBOSS Transeq	[80]	http://emboss.sourceforge.net/apps/release/6.6/emboss/apps/transeq.html
MUSCLE v3.5	[81]	http://www.drive5.com/muscle/muscle.html
IQtree	[85,86]	http://www.iqtree.org/

TrimAl	[83]	http://trimal.cgenomics.org/
FigTree	[87]	http://tree.bio.ed.ac.uk/software/figtree/
Trimmomatic v0.33	[88]	http://www.usadella.org/cms/?page=trimmomatic
SPAdes	[89]	https://cab.spbu.ru/software/spades/
L_RNA_Scaffolder	[90]	https://github.com/CYPRUS-Bioinformatics/L_RNA_scaffolder
PASA v2.0.2	[77]	https://github.com/PASAPipeline/PASApipeline
CEGMA	[91]	http://korflab.ucdavis.edu/datasets/cegma/
BUSCO	[92]	https://busco.ezlab.org/
RepeatMasker version open-4.0.6	[76]	http://www.repeatmasker.org/
AUGUSTUS v3.2.1	[78]	https://github.com/norbertz/nextgenusfs/augustus

486 **Acknowledgements**

487

488 We thank Dana Price and Debashish Bhattacharya (Rutgers University) for sequencing and preliminary
489 analysis of the genome data, and Mike Thang (QFAB, Australia) for support in submitting sequence data
490 to ENA. We thank the Osprey Ranch for supporting our writing retreats.

491

492 **Funding**

493

494 C.X.C. was supported by Australian Research Council grants (DP150101875 and DP190102474). P.M.
495 was supported by Natural Sciences and Engineering Research Council (NSERC) Discovery Grants
496 (RGPIN 356403-09; 2014-06288; 2019-06240). K.H. and M.L. were supported by the Hakai Institute.
497 J.X. was supported by the UBC Summer Undergraduate Research award, NSERC Graduate Student
498 fellowship and Patrick David Campbell Graduate Student fellowship. K.H. was supported by a
499 postdoctoral scholarship from the Tula Foundation.

500

501 **Author Contributions**

502

503 Conceptualization, J.X., K.H., and P.T.M.; Methodology, J.X., K.H., M.A.L., C.X.C.; Investigation, A.M.,
504 J.X., K.H., M.A.L., C.X.C.; Visualization, J.X., E.J.; Writing - Original Draft, J.X. and P.T.M.; Review
505 and Editing, J.X., K.H., M.A.L., E.J., C.X.C., P.T.M.; Funding Acquisition, P.T.M.; Supervision, P.T.M.

506

507 **Declaration of Interests**

508

509 The authors declare no competing interests.

510

511 **References**

512

- 513 1. Adey WH. The algal ridges and coral reefs of St. Croix: their structure and Holocene
514 development. *Atoll Research Bulletin*. 1975; 1–67. doi:<https://doi.org/10.5479/si.00775630.187.1>
- 515 2. Borowitzka MA. Algal calcification. *Oceanography and Marine Biology Annual Review*. 1977;
516 189–223.
- 517 3. Goreau TF. Calcium carbonate deposition by coralline algae and corals in relation to their roles as
518 reef-builders. *Annals of the New York Academy of Sciences*. 1963;109: 127–167.
- 519 4. Harrington L, Fabricius K, De’ath G, Negri A. Recognition and selection of settlement substrata
520 determine post-settlement survival in corals. *Ecology*. 2004;85: 3428–3437. doi:10.1890/04-0298
- 521 5. O’Leary JK, Barry JP, Gabrielson PW, Rogers-Bennett L, Potts DC, Palumbi SR, et al. Calcifying
522 algae maintain settlement cues to larval abalone following algal exposure to extreme ocean
523 acidification. *Scientific reports*. 2017;7: 5710–5774. doi:10.1038/s41598-017-05502-x
- 524 6. Swanson RL, de Nys R, Huggett MJ, Green JK, Steinberg PD. In situ quantification of a natural
525 settlement cue and recruitment of the Australian sea urchin *Holopneustes purpurascens*. *Marine*
526 *ecology Progress series (Halstenbek)*. 2006;314: 1–14. doi:10.3354/meps314001
- 527 7. Fisher K, Martone PT. Field study of growth and calcification rates of three species of articulated
528 coralline algae in British Columbia, Canada. *Biological Bulletin*. 2014;226: 121–130.
529 doi:10.1086/BBLv226n2p121
- 530 8. van der Heijden LH, Kamenos NA. Reviews and syntheses: Calculating the global contribution of
531 coralline algae to total carbon burial. *Biogeosciences*. 2015;12: 6429–6441. doi:10.5194/bg-12-
532 6429-2015
- 533 9. Gabrielson PW, Hughey JR, Diaz-Pulido G. Genomics reveals abundant speciation in the coral
534 reef building alga *Porolithon onkodes* (Corallinales, Rhodophyta). *Journal of phycology*. 2018;54:
535 429–434. doi:10.1111/jpy.12761
- 536 10. Hind KR, Miller KA, Young M, Jensen C, Gabrielson PW, Martone PT. Resolving cryptic species
537 of *Bossiella* (Corallinales, Rhodophyta) using contemporary and historical DNA. *American*

- 538 journal of botany. 2015;102: 1912–1930. doi:10.3732/ajb.1500308
- 539 11. Hind KR, Gabrielson PW, Lindstrom SC, Martone PT. Misleading morphologies and the
540 importance of sequencing type specimens for resolving coralline taxonomy (Corallinales,
541 Rhodophyta): *Pachyarthron cretaceum* is *Corallina officinalis*. Journal of Phycology. 2014;50:
542 760–764. doi:10.1111/jpy.12205
- 543 12. Twist BA, Neill KF, Bilewicz J, Jeong SY, Sutherland JE, Nelson WA. High diversity of
544 coralline algae in New Zealand revealed: Knowledge gaps and implications for future research.
545 PloS one. 2019;14: e0225645. doi:10.1371/journal.pone.0225645
- 546 13. Bergstrom E, Ordoñez A, Ho M, Hurd C, Fry B, Diaz-Pulido G. Inorganic carbon uptake
547 strategies in coralline algae: Plasticity across evolutionary lineages under ocean acidification and
548 warming. Marine environmental research. 2020;161: 105–107.
549 doi:10.1016/j.marenvres.2020.105107
- 550 14. Cornwall CE, Comeau S, McCulloch MT. Coralline algae elevate pH at the site of calcification
551 under ocean acidification. Global change biology. 2017;23: 4245–4256. doi:10.1111/gcb.13673
- 552 15. Guenther R. The effect of temperature and pH on the growth and biomechanics of coralline algae.
553 University of British Columbia. 2016.
- 554 16. McCoy SJ, Ragazzola F. Skeletal trade-offs in coralline algae in response to ocean acidification.
555 Nature climate change. 2014;4: 719–723. doi:10.1038/nclimate2273
- 556 17. Noisette F, Egilsdottir H, Davoult D, Martin S. Physiological responses of three temperate
557 coralline algae from contrasting habitats to near-future ocean acidification. Journal of
558 experimental marine biology and ecology. 2013;448: 179–187. doi:10.1016/j.jembe.2013.07.006
- 559 18. Hind KR, Gabrielson PW, Jensen C, Martone PT. Evolutionary reversals in *Bossiella*
560 (Corallinales, Rhodophyta): first report of a coralline genus with both geniculate and
561 nongeniculate species. Journal of phycology. 2018;54: 788–798. doi:10.1111/jpy.12788
- 562 19. Janot K, Martone PT. Convergence of joint mechanics in independently evolving, articulated
563 coralline algae. Journal of experimental biology. 2016;219: 383–391. doi:10.1242/jeb.131755

- 564 20. Steneck RS. The ecology of coralline algal crusts: convergent patterns and adaptive strategies.
565 Ann Rev Ecol Syst. 1986;17: 273–303.
- 566 21. Aguirre J, Perfectti F, Braga JC. Integrating phylogeny , molecular clocks , and the fossil record in
567 the evolution of coralline algae (Corallinales and Sporolithales , Rhodophyta) Author (s): Julio
568 Aguirre , Francisco Perfectti and Juan C . Braga Published by : Cambridge University P.
569 Paleobiology. 2010;36: 519–533.
- 570 22. Rösler A, Perfectti F, Peña V, Aguirre J, Braga JC, Gabrielson P. Timing of the evolutionary
571 history of Corallinaceae (Corallinales, Rhodophyta). Journal of Phycology. 2017;53: 567–576.
572 doi:10.1111/jpy.12520
- 573 23. Martone PT, Estevez JM, Lu F, Ruel K, Denny MW, Somerville C, et al. Discovery of Lignin in
574 Seaweed Reveals Convergent Evolution of Cell-Wall Architecture. Current Biology. 2009;19:
575 169–175. doi:10.1016/j.cub.2008.12.031
- 576 24. Boerjan W, Ralph J, Baucher M. Lignin Biosynthesis. Annual Review of Plant Biology. 2003;54:
577 519–546. doi:10.1146/annurev.arplant.54.031902.134938
- 578 25. Mottiar Y, Vanholme R, Boerjan W, Ralph J, Mansfield SD. Designer lignins: Harnessing the
579 plasticity of lignification. Current Opinion in Biotechnology. 2016;37: 190–200.
580 doi:10.1016/j.copbio.2015.10.009
- 581 26. Vanholme R, Demedts B, Morreel K, Ralph J, Boerjan W. Lignin biosynthesis and structure. Plant
582 Physiology. 2010;153: 895–905. doi:10.1104/pp.110.155119
- 583 27. Lange BM, Lapierre C, Sandermann H. Elicitor-induced spruce stress lignin: Structural similarity
584 to early developmental lignins. Plant Physiology. 1995;108: 1277–1287.
585 doi:10.1104/pp.108.3.1277
- 586 28. Tronchet M, BalaguÉ C, Kroj T, Jouanin L, Roby D. Cinnamyl alcohol dehydrogenases-C and D,
587 key enzymes in lignin biosynthesis, play an essential role in disease resistance in Arabidopsis.
588 Molecular Plant Pathology. 2010;11: 83–92. doi:10.1111/j.1364-3703.2009.00578.x
- 589 29. Martone PT. Kelp versus coralline: Cellular basis for mechanical strength in the wave-swept

- 590 seaweed Calliarthron (Corallinaceae, Rhodophyta). *Journal of Phycology*. 2007;43: 882–891.
591 doi:10.1111/j.1529-8817.2007.00397.x
- 592 30. Denny MW, King FA. The extraordinary joint material of an articulated coralline alga. II.
593 Modeling the structural basis of its mechanical properties. *Journal of Experimental Biology*.
594 2016;219: 1843–1850. doi:10.1242/jeb.138867
- 595 31. Weng JK, Chapple C. The origin and evolution of lignin biosynthesis. *New Phytologist*. 2010;187:
596 273–285. doi:10.1111/j.1469-8137.2010.03327.x
- 597 32. Dixon RA, Barros J. Lignin biosynthesis: Old roads revisited and new roads explored. *Open*
598 *Biology*. 2019;9. doi:10.1098/rsob.190215
- 599 33. Raes, J., Rohde, A., Christensen, J. H., Van de Peer, Y., Boerjan W. Genome-Wide
600 Characterization of the Lignification Toolbox in Arabidopsis. *Plant Physiology*. 2014;133: 1051–
601 1071. doi:10.1104/pp.103.026484.role
- 602 34. Weng JK, Akiyama T, Bonawitz ND, Li X, Ralph J, Chapple C. Convergent evolution of syringyl
603 lignin biosynthesis via distinct pathways in the lycophyte *Selaginella* and flowering plants. *Plant*
604 *Cell*. 2010;22: 1033–1045. doi:10.1105/tpc.109.073528
- 605 35. Weng J-K, Li X, Stout J, Chapple C. Independent origins of syringyl lignin in vascular plants.
606 *Proceedings of the National Academy of Sciences*. 2008;105: 7887 LP – 7892.
607 doi:10.1073/pnas.0801696105
- 608 36. Labeeuw L, Martone PT, Boucher Y, Case RJ. Ancient origin of the biosynthesis of lignin
609 precursors. *Biology Direct*. 2015;10: 1–21. doi:10.1186/s13062-015-0052-y
- 610 37. Matsuzaki M, Misumi O, Shin-i T, Maruyama S, Takahara M, Miyagishima S, et al. Genome
611 sequence of the ultrasmall unicellular red alga *Cyanidioschyzon merolae* 10D. *Nature*. 2004;428:
612 653–657. doi:10.1038/nature02398
- 613 38. Collén J, Porcel B, Carré W, Ball SG, Chaparro C, Tonon T, et al. Genome structure and
614 metabolic features in the red seaweed *Chondrus crispus* shed light on evolution of the
615 Archaeplastida. *Proceedings of the National Academy of Sciences of the United States of*

- 616 America. 2013;110: 5247–5252. doi:10.1073/pnas.1221259110
- 617 39. Brawley SH, Blouin NA, Ficko-Blean E, Wheeler GL, Lohr M, Goodson H V., et al. Insights into
618 the red algae and eukaryotic evolution from the genome of *Porphyra umbilicalis* (Bangiophyceae,
619 Rhodophyta). *Proceedings of the National Academy of Sciences of the United States of America*.
620 2017;114: E6361–E6370. doi:10.1073/pnas.1703088114
- 621 40. Lee JM, Yang EC, Graf L, Yang JH, Qiu H, Zelzion U, et al. Analysis of the draft genome of the
622 red seaweed *Gracilaria lemaneiformis* provides insights into genome size evolution in rhodophyta.
623 *Molecular Biology and Evolution*. 2018;35: 1869–1886. doi:10.1093/molbev/msy081
- 624 41. Page TM, McDougall C, Diaz-Pulido G. De novo transcriptome assembly for four species of
625 crustose coralline algae and analysis of unique orthologous genes. *Scientific Reports*. 2019;9.
626 doi:10.1038/s41598-019-48283-1
- 627 42. Bi G, Liu G, Zhao E, Du Q. Complete mitochondrial genome of a red calcified alga *Calliarthron*
628 *tuberculosum* (Corallinales). *Mitochondrial DNA*. 2016;27: 2554–2556.
629 doi:10.3109/19401736.2015.1038801
- 630 43. Chan CX, Yang EC, Banerjee T, Yoon HS, Martone PT, Estevez JM, et al. Red and green algal
631 monophyly and extensive gene sharing found in a rich repertoire of red algal genes. *Current*
632 *Biology*. 2011;21: 328–333. doi:10.1016/j.cub.2011.01.037
- 633 44. Shockey JM, Fulda MS, Browse J. Arabidopsis Contains a Large Superfamily of Acyl-Activating
634 Enzymes . Phylogenetic and Acyl-Coenzyme A Synthetases 1. *Plant physiology*. 2003;132: 1065–
635 1076. doi:10.1104/pp.103.020552.ularly
- 636 45. Shockey J, Browse J. Genome-level and biochemical diversity of the acyl-activating enzyme
637 superfamily in plants. *Plant Journal*. 2011;66: 143–160. doi:10.1111/j.1365-313X.2011.04512.x
- 638 46. Li L, Cheng XF, Leshkevich J, Umezawa T, Harding SA, Chiang VL. The Last Step of Syringyl
639 Monolignol Biosynthesis in Angiosperms Is Regulated by a Novel Gene Encoding Sinapyl
640 Alcohol Dehydrogenase. *The Plant Cell*. 2001;13: 1567–1586. doi:10.1105/tpc.010111
- 641 47. Hofmann LC, Schoenrock K, de Beer D. Arctic Coralline Algae Elevate Surface pH and

- 642 Carbonate in the Dark. *Frontiers in plant science*. 2018;9: 1416. doi:10.3389/fpls.2018.01416
- 643 48. Nam O, Shiraiwa Y, Jin E. Calcium-related genes associated with intracellular calcification of
644 *Emiliana huxleyi* (Haptophyta) CCMP 371. *ALGAE*. 2018;33: 181–189.
645 doi:10.4490/algae.2018.33.4.21
- 646 49. Xue J, Purushotham P, Acheson JF, Ho R, Zimmer J, McFarlane C, et al. Functional
647 characterization of a cellulose synthase, CtCESA1, from the marine red alga *Calliarthron*
648 *tuberculosis* (Corallinales). *Journal of Experimental Botany*. 2021; erab414.
649 doi:10.1093/jxb/erab414
- 650 50. Kyndt JA, Meyer TE, Cusanovich MA, Van Beeumen JJ. Characterization of a bacterial tyrosine
651 ammonia lyase, a biosynthetic enzyme for the photoactive yellow protein. *FEBS letters*. 2002;512:
652 240–244. doi:10.1016/S0014-5793(02)02272-X
- 653 51. Barros J, Serrani-Yarce JC, Chen F, Baxter D, Venables BJ, Dixon RA. Role of bifunctional
654 ammonia-lyase in grass cell wall biosynthesis. *Nature plants*. 2016;2: 16050.
655 doi:10.1038/nplants.2016.50
- 656 52. Cooke HA, Christianson C V, Bruner SD. Structure and chemistry of 4-methylideneimidazole-5-
657 one containing enzymes. *Current opinion in chemical biology*. 2009;13: 460–468.
658 doi:10.1016/j.cbpa.2009.06.013
- 659 53. Mohy El-Din SM, El-Ahwany AMD. Bioactivity and phytochemical constituents of marine red
660 seaweeds (*Jania rubens*, *Corallina mediterranea* and *Pterocladia capillacea*). *Journal of Taibah*
661 *University for Science*. 2016;10: 471–484. doi:<https://doi.org/10.1016/j.jtusci.2015.06.004>
- 662 54. Mallinson SJB, Machovina MM, Silveira RL, Garcia-Borràs M, Gallup N, Johnson CW, et al. A
663 promiscuous cytochrome P450 aromatic O-demethylase for lignin bioconversion. *Nature*
664 *communications*. 2018;9: 2412–2487. doi:10.1038/s41467-018-04878-2
- 665 55. Guo J, Ma X, Cai Y, Ma Y, Zhan Z, Zhou YJ, et al. Cytochrome P450 promiscuity leads to a
666 bifurcating biosynthetic pathway for tanshinones. *The New phytologist*. 2016;210: 525–534.
667 doi:10.1111/nph.13790

- 668 56. Hoffmann L, Besseau S, Geoffroy P, Ritzenthaler C, Meyer D, Lapierre C, et al. Silencing of
669 Hydroxycinnamoyl-Coenzyme A Shikimate/Quinate Hydroxycinnamoyltransferase Affects
670 Phenylpropanoid Biosynthesis. *The Plant cell*. 2004;16: 1446–1465. doi:10.1105/tpc.020297
- 671 57. Goujon T, Sibout R, Pollet B, Maba B, Nussaume L, Bechtold N, et al. A new *Arabidopsis*
672 *thaliana* mutant deficient in the expression of O-methyltransferase impacts lignins and sinapoyl
673 esters. *Plant Molecular Biology*. 2003;51: 973–989. doi:10.1023/A:1023022825098
- 674 58. Lu F, Marita JM, Lapierre C, Jouanin L, Morreel K, Boerjan W, et al. Sequencing around 5-
675 Hydroxyconiferyl Alcohol-Derived Units in Caffeic Acid O -Methyltransferase-Deficient Poplar
676 Lignins. *Plant physiology (Bethesda)*. 2010;153: 569–579. doi:10.1104/pp.110.154278
- 677 59. Guo D, Chen F, Inoue K, Blount JW, Dixon RA. Downregulation of Caffeic Acid 3- O -
678 Methyltransferase and Caffeoyl CoA 3- O -Methyltransferase in Transgenic Alfalfa: Impacts on
679 Lignin Structure and Implications for the Biosynthesis of G and S Lignin. *The Plant cell*. 2001;13:
680 73–88. doi:10.1105/tpc.13.1.73
- 681 60. Li L, Popko JL, Zhang X-H, Osakabe K, Tsai C-J, Joshi CP, et al. A Novel Multifunctional O-
682 Methyltransferase Implicated in a Dual Methylation Pathway Associated with Lignin Biosynthesis
683 in Loblolly Pine. *Proceedings of the National Academy of Sciences - PNAS*. 1997;94: 5461–5466.
684 doi:10.1073/pnas.94.10.5461
- 685 61. Hu Y, Gai Y, Yin L, Wang X, Feng C, Feng L, et al. Crystal Structures of a *Populus tomentosa* 4-
686 Coumarate : CoA Ligase Shed Light on Its Enzymatic Mechanisms. *Plant physiology*. 2010;22:
687 3093–3104. doi:10.1105/tpc.109.072652
- 688 62. Witzel K, Schomburg D, Kombrink E, Schneider K, Ho K, Stuible H. The substrate specificity-
689 determining amino acid code of 4-coumarate : CoA ligase. *PNAS*. 2003;100: 8601–8606.
- 690 63. Stuible H, Kombrink E. Identification of the Substrate Specificity-conferring Amino Acid
691 Residues of 4-Coumarate : Coenzyme A Ligase Allows the Rational Design of Mutant Enzymes
692 with New Catalytic Properties. *Journal of Biological Chemistry*. 2001;276: 26893–26897.
693 doi:10.1074/jbc.M100355200

- 694 64. Jörnvall H, Persson B, Krook M, Atrian S, González-Duarte R, Jeffery J, et al. Short-Chain
695 Dehydrogenases/Reductases (SDR). *Biochemistry*. 1995;34: 6003–6013.
696 doi:10.1021/bi00018a001
- 697 65. Sattler SA, Walker AM, Vermerris W, Sattler SE, Kang C. Structural and Biochemical
698 Characterization of Cinnamoyl-CoA Reductases. *Plant physiology*. 2017;173: 1031–1044.
699 doi:10.1104/pp.16.01671
- 700 66. Filling C, Berndt KD, Benach J, Knapp S, Prozorovski T, Nordling E, et al. Critical Residues for
701 Structure and Catalysis in Short-chain Dehydrogenases / Reductases. *Biological Chemistry*.
702 2002;277: 25677–25684. doi:10.1074/jbc.M202160200
- 703 67. Bukh C, Nord-Larsen PH, Rasmussen SK. Phylogeny and structure of the cinnamyl alcohol
704 dehydrogenase gene family in *Brachypodium distachyon*. *Journal of Experimental Botany*.
705 2012;63: 6223–6236. doi:10.1093/jxb/ers275
- 706 68. Youn B, Camacho R, Moinuddin SGA, Lee C, Davin LB, Lewis NG, et al. Crystal structures and
707 catalytic mechanism of the *Arabidopsis* cinnamyl alcohol dehydrogenases AtCAD5 and AtCAD4.
708 *Organic & Biomolecular Chemistry*. 2006;4: 1687–1697. doi:10.1039/B601672C
- 709 69. Bomati EK, Noel JP. Structural and kinetic basis for substrate selectivity in *Populus tremuloides*
710 sinapyl alcohol dehydrogenase. *The Plant cell*. 2005/04/13. 2005;17: 1598–1611.
711 doi:10.1105/tpc.104.029983
- 712 70. Julián-sánchez A, Riveros-rosas H, Piña E. Evolution of Cinnamyl Alcohol Dehydrogenase
713 Family Evolution of Cinnamyl Alcohol Dehydrogenase Family. In: Weiner H, Plapp B, Lindahl R,
714 Maser E, editors. *Enzymology and Molecular Biology of Carbonyl Metabolism*. West Lafayette:
715 Purdue University Press; 2006. pp. 142–153.
- 716 71. von Borzyskowski LS, Rosenthal RG, Erb TJ. Evolutionary history and biotechnological future of
717 carboxylases. *Journal of Biotechnology*. 2013;168: 243–251. doi:10.1016/j.jbiotec.2013.05.007
- 718 72. Haas BJ, Papanicolaou A, Yassour M, Grabherr M, Philip D, Bowden J, et al. De novo transcript
719 sequence reconstruction from RNA-Seq: reference generation and analysis with Trinity. *Nature*

- 720 protocols. 2013;8: 1–43. doi:10.1038/nprot.2013.084.De
- 721 73. Conesa A, Götz S, García-Gómez JM, Terol J, Talón M, Robles M. Blast2GO: A universal tool
722 for annotation, visualization and analysis in functional genomics research. *Bioinformatics*.
723 2005;21: 3674–3676. doi:10.1093/bioinformatics/bti610
- 724 74. Kanehisa M, Sato Y, Kawashima M, Furumichi M, Tanabe M. KEGG as a reference resource for
725 gene and protein annotation. *Nucleic acids research*. 2016;44: 457–462. doi:10.1093/nar/gkv1070
- 726 75. Luo W, Brouwer C. Pathview: an R/Bioconductor package for pathway-based data integration and
727 visualization. *Computer applications in the biosciences*. 2013;29: 1830–1831.
728 doi:10.1093/bioinformatics/btt285
- 729 76. Smit A, Hubley R, Green P. RepeatMasker Open-4.0.
- 730 77. Haas BJ, Delcher AL, Mount SM, Wortman JR, Smith RK, Hannick LI, et al. Improving the
731 Arabidopsis genome annotation using maximal transcript alignment assemblies. *Nucleic Acids*
732 *Research*. 2003;31: 5654–5666. doi:10.1093/nar/gkg770
- 733 78. Stanke M, Schöffmann O, Morgenstern B, Waack S. Gene prediction in eukaryotes with a
734 generalized hidden Markov model that uses hints from external sources. *BMC Bioinformatics*.
735 2006;7: 1–11. doi:10.1186/1471-2105-7-62
- 736 79. Finn RD, Clements J, Eddy SR. HMMER Web Server: Interactive Sequence Similarity Searching.
737 *Nucleic Acids Research*. 2011;39: W29–W37. doi:10.1093/nar/gkr367
- 738 80. Rice P, Longden I, Bleasby A. EMBOSS: The European Molecular Biology Open Software Suite.
739 *Trends in Genetics*. 2000;16: 276–277. doi:10.1016/S0168-9525(00)02024-2
- 740 81. Edgar RC. MUSCLE: a Multiple Sequence Alignment Method With Reduced Time and Space
741 Complexity. *BMC Bioinformatics*. 2004;5. doi:10.1186/1471-2105-5-113
- 742 82. Mahram A, Herbordt MC. Fast and Accurate NCBI BLASTP: Acceleration with Multiphase
743 FPGA-based Prefiltering. *Proceedings of the 24th ACM International Conference on*
744 *Supercomputing*. New York, NY, USA: ACM; 2010. pp. 73–82. doi:10.1145/1810085.1810099
- 745 83. Capella-Gutiérrez S, Silla-Martínez JM, Gabaldón T. trimAl: a tool for automated alignment

- 746 trimming in large-scale phylogenetic analyses. *Bioinformatics*. 2009/06/08. 2009;25: 1972–1973.
747 doi:10.1093/bioinformatics/btp348
- 748 84. Luo A, Qiao H, Zhang Y, Shi W, Ho SY, Xu W, et al. Performance of criteria for selecting
749 evolutionary models in phylogenetics: a comprehensive study based on simulated datasets. *BMC*
750 *evolutionary biology*. 2010;10: 242. doi:10.1186/1471-2148-10-242
- 751 85. Nguyen L-T, Schmidt HA, von Haeseler A, Minh BQ. IQ-TREE: A Fast and Effective Stochastic
752 Algorithm for Estimating Maximum-Likelihood Phylogenies. *Molecular Biology and Evolution*.
753 2015;32: 268–274.
- 754 86. Hoang DT, Chernomor O, von Haeseler A, Minh BQ, Vinh LS. UFBoot2: Improving the Ultrafast
755 Bootstrap Approximation. *Molecular Biology and Evolution*. 2018;35: 518–522.
- 756 87. Rambaut A, Drummond A. FigTree v1. 3.1 Institute of Evolutionary Biology. University of
757 Edinburgh. 2010.
- 758 88. Bolger AM, Lohse M, Usadel B. Trimmomatic: A flexible trimmer for Illumina sequence data.
759 *Bioinformatics*. 2014;30: 2114–2120. doi:10.1093/bioinformatics/btu170
- 760 89. Bankevich A, Nurk S, Antipov D, Gurevich AA, Dvorkin M, Kulikov AS, et al. SPAdes: A new
761 genome assembly algorithm and its applications to single-cell sequencing. *Journal of*
762 *Computational Biology*. 2012;19: 455–477. doi:10.1089/cmb.2012.0021
- 763 90. Xue W, Li JT, Zhu YP, Hou GY, Kong XF, Kuang YY, et al. L_RNA_scaffolder: Scaffolding
764 genomes with transcripts. *BMC Genomics*. 2013;14: 1–14. doi:10.1186/1471-2164-14-604
- 765 91. Parra G, Bradnam K, Korf I. CEGMA: A pipeline to accurately annotate core genes in eukaryotic
766 genomes. *Bioinformatics*. 2007;23: 1061–1067. doi:10.1093/bioinformatics/btm071
- 767 92. Simão FA, Waterhouse RM, Ioannidis P, Kriventseva E V., Zdobnov EM. BUSCO: Assessing
768 genome assembly and annotation completeness with single-copy orthologs. *Bioinformatics*.
769 2015;31: 3210–3212. doi:10.1093/bioinformatics/btv351
- 770
771

772 **Supporting Information**

773

774 **Fig S1. Completeness of the *C. tuberculosis* transcriptome dataset.**

775 **(A)** Transcriptome sequences show high recovery of eukaryotic genes in CEGMA/BUSCO analysis.

776 Percentage of genomic scaffolds with transcriptome support and transcriptomic scaffolds alone that share
777 amino acid sequences with the core eukaryotic gene databases including CEGMA, BUSCO eukaryotic,
778 and BUSCO Viridiplantae. Transcriptome encoded amino acid sequences were searched against the
779 databases using BLASTP (orange) or TBLASTN (yellow), and genomic scaffolds were searched against
780 the databases using TBLASTN (blue)

781 **(B)** Transcriptomic support of genomic data analyzed by GC content and transcript length.

782 The distribution of GC content (above) against transcript lengths is shown for scaffolds with
783 transcriptome support (blue) and scaffolds without transcriptome support (yellow) (right).

784 **Fig S2. C3H, C4H, F5H, P450 candidates from *C. tuberculosis* in relation to plants and other taxa.**

785 **(A)** Partial alignment of *C. tuberculosis* P450 candidates with C3H, C4H, and F5H from *A. thaliana*,
786 and a novel F5H from *Selaginella moellendorffii*. Heme binding domain residues, secondary structure
787 stabilizing K helix residues, PXX, and the I-helix are indicated [8]. Sites with <80% coverage were
788 removed. A strong candidate for beta-carotene synthesis is indicated with a triangle.

789 **(B)** Unrooted CYP450 maximum likelihood gene tree with *C. tuberculosis* (magenta dots) and
790 additional taxa (Embryophyta – dark green, Chlorophyta – light green, Rhodophyta – red, Animalia and
791 Opisthokonta – purple, Bacteria and Cyanobacteria – blue, Oomycota, Mycetozoa and Fungi – yellow,
792 Ochrophyta – brown). Functionally demonstrated plant C3H, C4H, and F5H are labeled (+). Additional
793 functional groups are labeled [9]. Ultrafastbootstrap values > 95 are marked by *. Model = VT+F+G4.

794

795 **Fig S3. CCoAOMT candidates from *C. tuberculosis* in relation to plants and other taxa.**

796 **(A)** Partial alignment of *C. tuberculosis* CCoAOMT sequence candidates with CCoAOMT from land
797 plants. Substrate recognition residues (black triangle), divalent metal ion and cofactor binding residues
798 (grey triangle), catalytic residues (back square), and the positively charged R220 necessary for substrate
799 recognition (grey square) are indicated. Sites with < 70% coverage were removed.

800 **(B)** Unrooted maximum likelihood gene tree of biochemically characterized plant O-methyltransferases
801 with *C. tuberculosis* (magenta dots) and additional taxa (Embryophyta – dark green, Chlorophyta – light
802 green, Rhodophyta – red, Animalia and Opisthokonta – purple, Bacteria and Cyanobacteria – blue,
803 Oomycota, Mycetozoa and Fungi – yellow, Ochrophyta – brown). Functionally demonstrated plant

804 CCoAOMT are labeled (+). Additional functional groups are labeled [13]. Ultrafastbootstrap values > 95
805 are marked by *. Model = LG + G4. JMT, SAMT, and BAMT are closely related to OMTs.

806

807 **Fig S4. CSE candidates from *C. tuberculosis* in relation to plants and other taxa.**

808 (A) Partial alignment of *C. tuberculosis* CSE sequence candidates with CSE from land plants. Acyl
809 transferase motifs (HX₄D), lipase motifs (GX₄SXG) and active site residues (triangle) are indicated. Sites
810 with < 70% coverage were removed.

811 (B) Unrooted maximum likelihood gene tree of *C. tuberculosis* CSE candidates (magenta dots) and
812 additional taxa (Embryophyta – dark green, Chlorophyta – light green, Rhodophyta – red, Animalia and
813 Opisthokonta – purple, Bacteria and Cyanobacteria – blue, Oomycota, Mycetozoa and Fungi – yellow,
814 Ochrophyta – brown). Functionally demonstrated plant CSE are labeled (+). Additional functional groups
815 are labeled. Ultrafastbootstrap values > 95 are marked by *. Model = VT+G4.

816

817 **Fig. S5. A visual representation of the *C. tuberculosis* sequences present in the starch and sucrose
818 metabolism pathway from the KEGG based annotation.**

819 KEGG based annotation showing the starch and sucrose metabolic pathway with *C. tuberculosis*
820 annotations highlighted. The gradient map in the top right corner indicates the level of transcription, with
821 white and dark pink coloring representing absence and presence of expression respectively. The annotated
822 map, number “00500”, was extracted in the provided R file using the pathview program.

823

824 **Table S1. Summary statistics for the *C. tuberculosis* genome assembly.**

825 Scaffolds are categorized as shared with either red algal (*Pyropia yezoensis*) genomic scaffolds,
826 eukaryotic sequences, or other bacteria sequences based on sequence similarity.

827 **Table S2. Top hits against *Arabidopsis thaliana* (taxid:3702) using *Calliarthron* sequences as the**

828 **search query (BLASTP).** Query sequence is indicated by contig number. Result hits are indicated by
829 description (At tax ID 3702) and colored by overall alignment scores with red (≥ 200), pink (80-200),
830 green (50-80), blue (40-50), and black (<40) that are most to least reliable scores in that order.

831

832 **Table S3. KEGG annotations of *Calliarthron tuberculosis* reads from the combined transcriptomic**

833 **dataset.** Unique reads are represented by their contig identifier (contig_gene_isoform) and matched with
834 their annotated KEGG based identifier (KO_identifier) and associated protein name.

835

836 **Table S4. Listed representation of the *C. tuberculosis* sequences present in starch and sucrose**
837 **metabolism pathway from the KEGG based annotation.**

838 *C. tuberculosis* sequences were extracted from the KEGG based starch and sucrose metabolism pathway
839 number “00500”. “KEGG Identifier” refers to the specific KEGG code for the gene, “Contig Name”
840 refers to the sequence identifier from the *Calliathron* transcriptome where the values represent the contig
841 name_gene number_gene isoform and “Gene Name” refers to the gene acronym, the gene name, and its
842 enzyme commission (EC) number. Sequences were extracted in the provided R file using the pathview
843 program.

844

845 **Table S5. A list of calcification related gene candidates identified from KEGG-based annotations of**
846 **the *C. tuberculosis* transcriptome.**

847 Calcification gene candidates were initially selected based on a literature search, and then *C.*
848 *tuberculosis* sequences were identified manually from the KEGG based annotations (annotation file
849 available on Github), thus this is not an exhaustive list. The genes are organized by their functional
850 classification indicated as “overall function”, while “KEGG Identifier” refers to the specific KEGG code
851 for the gene, “Contig Name” refers to the sequence identifier from the *Calliathron* transcriptome where
852 the values represent the contig name_gene number_gene isoform and “Gene Name” refers to the gene
853 acronym, the gene name, and its enzyme commission (EC) number.

854

855

856

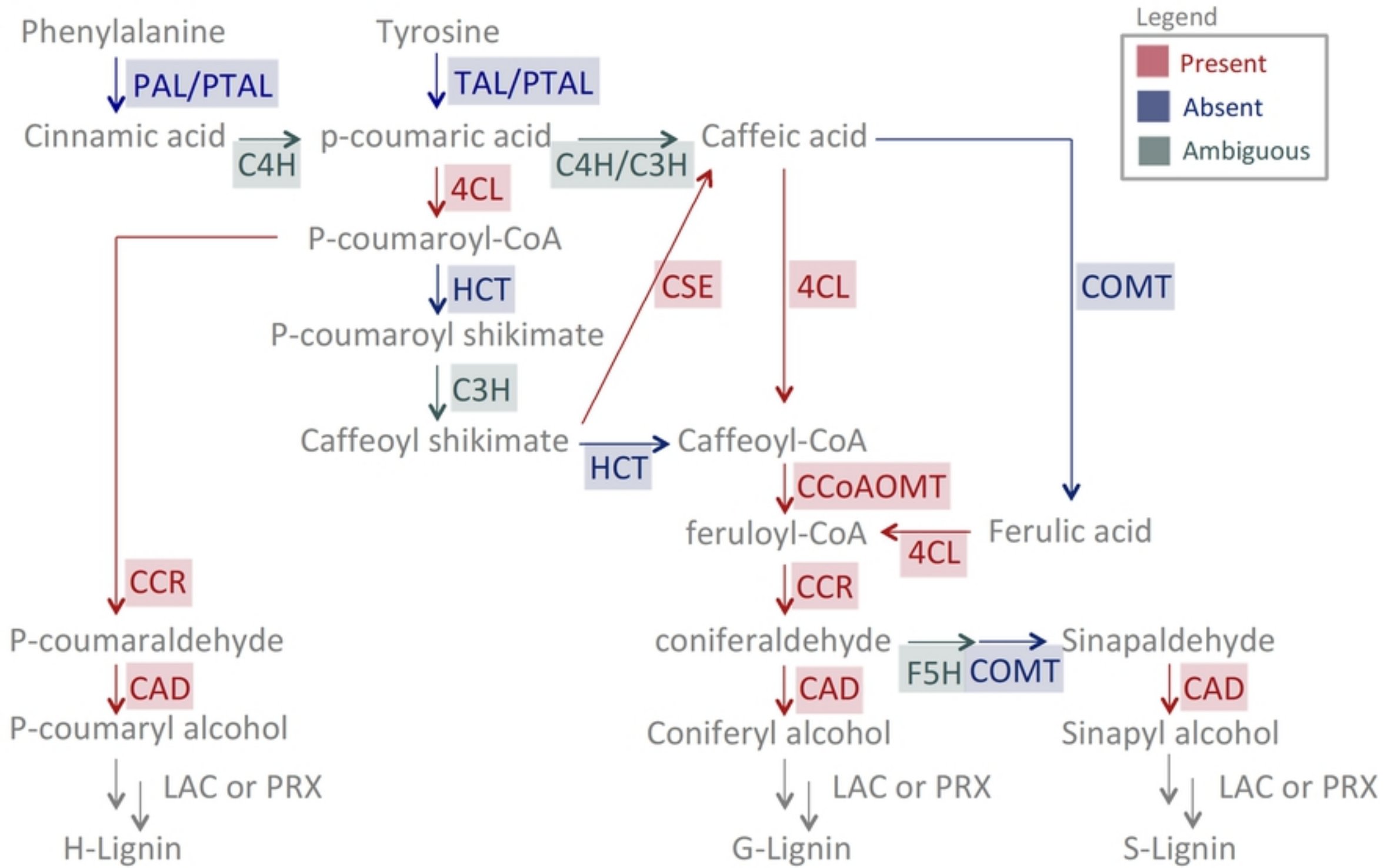
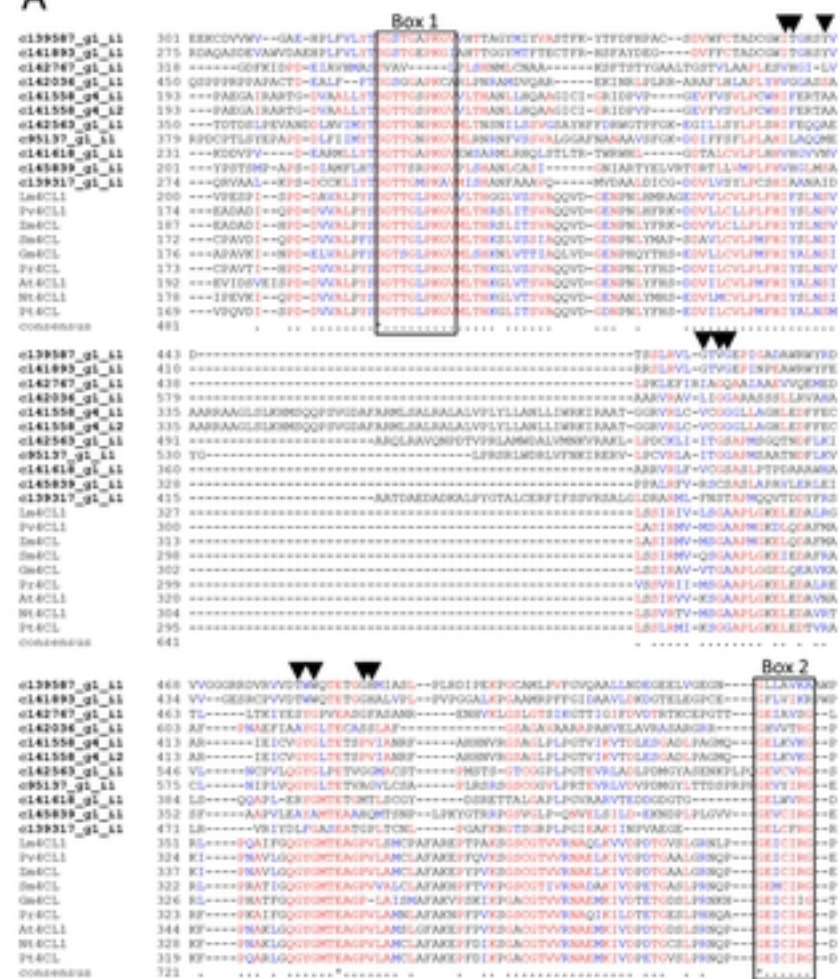


Figure 1

A



B

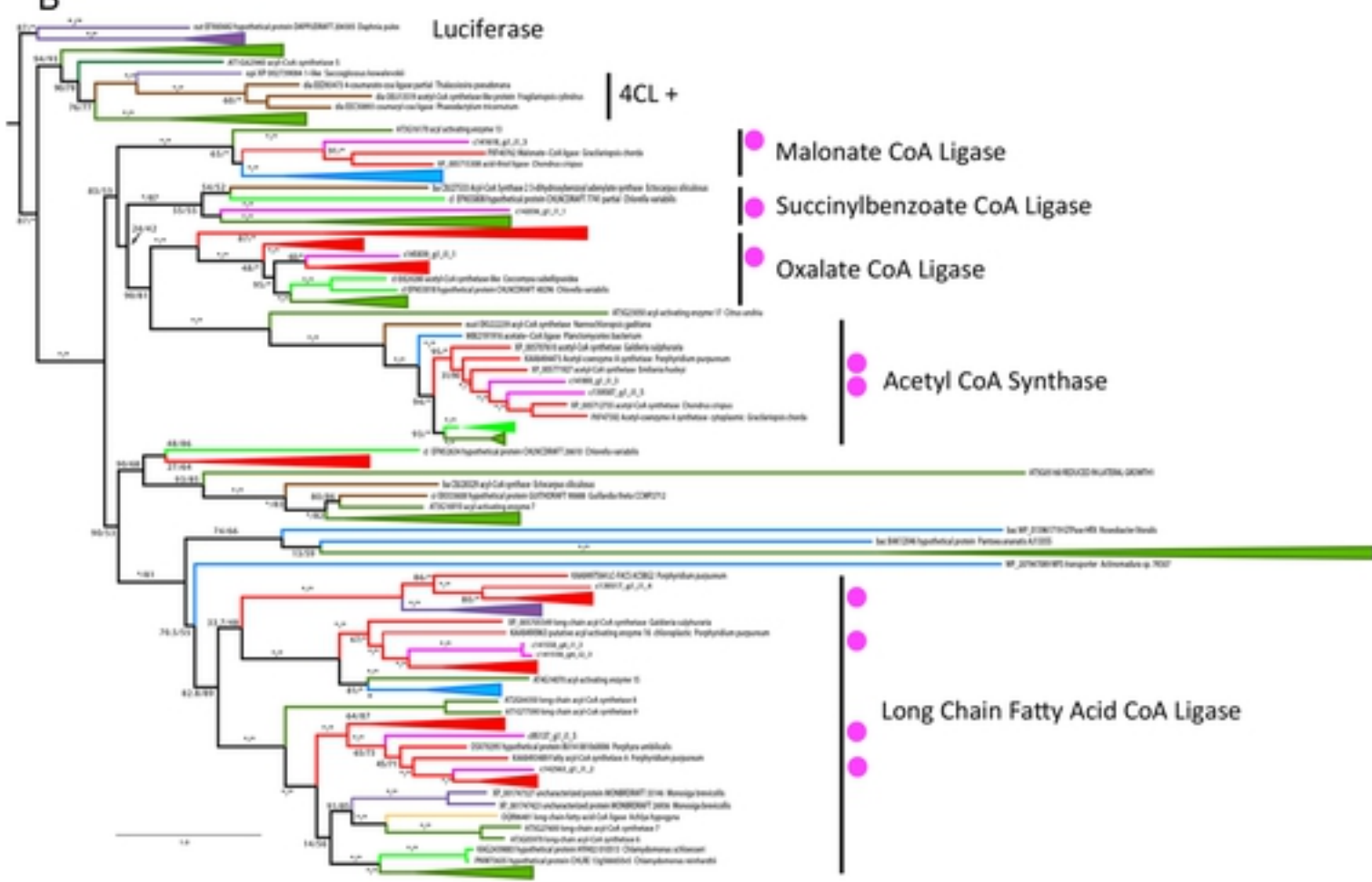
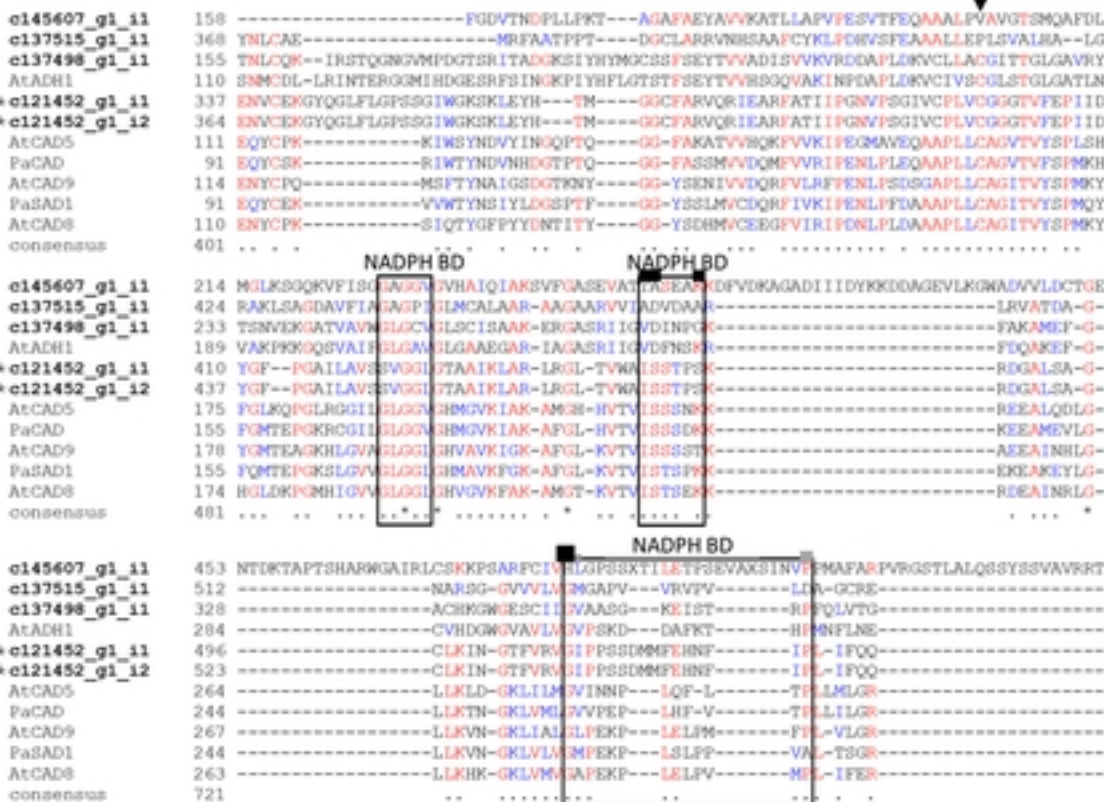


Figure 2

A



B

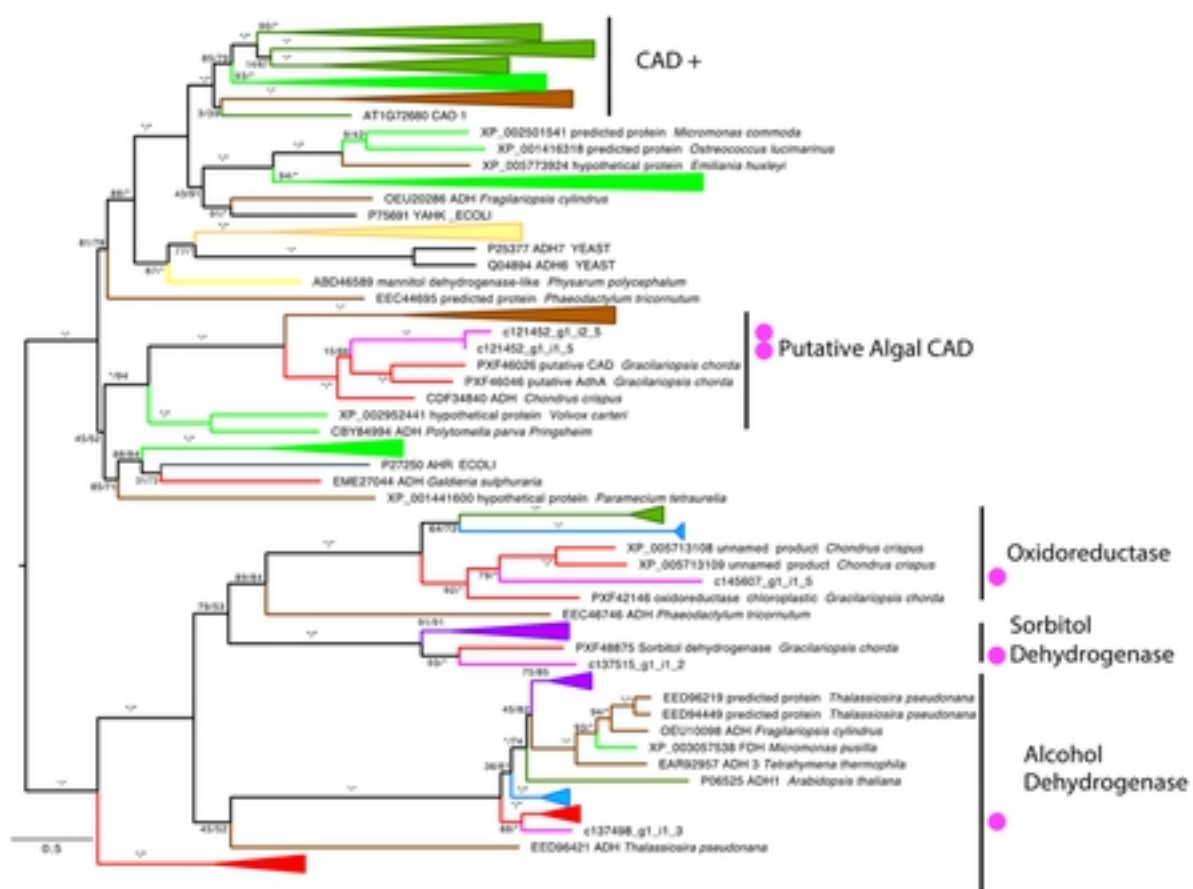


Figure 4